Supporting Information

Enhanced Exciton-phonon Coupling in Pseudohalide 2D Perovskite for X-ray to Visible Light Detection

1. Experimental section

Materials

Cesium iodide (CsI, 99.99%) and cesium bromide (CsBr, 99.99%) sourced from Xi'an Polymer Light Technology Co., lead thiocyanate ($Pb(SCN)_2$, 99.5%) from Innochem Technology Co., Ltd., dimethyl sulfoxide (DMSO, >99.8%) and tin dioxide (SnO_2) 15% hydrocolloid dispersion from Alfa Aesar, N,N-dimethylformamide (DMF, 99.99%) from TCI, polyvinylpyrrolidone (PVP) from Aladdin, and titanium tetrachloride ($TiCl_4$, 99.5%) from ACROS, were procured without further purification for use in the study.

Precursor preparation

The $Cs_2Pb(SCN)_2X_2$ (X = I and Br) perovskite precursor solutions were formulated by dissolving 0.5 mmol $Pb(SCN)_2$ and 1 mmol CsX (X = I and Br) in 1 mL anhydrous DMF/DMSO (3:7, v/v) solution, followed by stirring at 60 °C overnight. For the mixed I/Br systems, the corresponding ratios were employed, with all other processes remaining consistent. SnO_2 solutions were prepared by combining tin dioxide 15% hydrocolloid dispersion and deionized water in a 1:6 volume ratio.

Device fabrication

The glass substrates underwent sequential ultrasonic cleaning with deionized water, isopropanol, deionized water, and ethanol. After air-drying, the substrates underwent a 20-minute UV-O_3 treatment. The TiO_2 substrates were prepared by immersing the substrate in a $TiCl_4$ solution, heating it at 70 °C for 1 h, replacing the $TiCl_4$ solution with deionized water, and then heating the glass substrate at 200 °C for 1 h. The SnO_2 substrates were prepared by adding SnO_2 precursor solution to a glass substrate, spin-coating at 5000 rpm for 50 s, and annealing at 150 °C for 40 min to form the SnO_2 layer. Subsequently, the glass/TiO_2 (or SnO_2) substrate was preheated at 50 °C, and the perovskite precursor solution was filtered through a 0.22 μm filter head, followed by spin-coating at 3000 rpm for 30 s, and annealing at 80 °C for two minutes. Finally, a 60 nm gold interdigitated electrode (electrode distance: L = 50 μm) was deposited via thermal evaporation under 4×10^{-4} Pa. The effective area of the electrode is 7.25×10^{-3} cm^2.

Material characterization

Power X-ray diffraction (XRD) patterns were obtained using a Rigaku SmartLab X-ray diffractometer with Cu Kα radiation (0.15418 nm). Scanning electron microscope (SEM) images were captured utilizing a Hitachi High Technologies Co. SU8010. X-ray photoelectron spectra (XPS) were acquired employing a Thermo Fisher Scientific ESCALab250Xi spectrometer. UV-vis absorption spectra were measured using a Shimadzu UV2450 UV-vis spectrophotometer. Steady-state PL and temperature-dependent PL (TDPL) spectra were recorded using an Edinburgh FLS 1000 spectrometer under xenon lamp excitation. Excitation wavelengths were set at 400 nm and 530 nm for $Cs_2Pb(SCN)_2Br_2$ and $Cs_2Pb(SCN)_2I_2$, respectively. For TDPL measurements, samples were initially cooled to 113 K under 6.5×10^{-6} Pa and then heated in 20 K increments. The temperature was maintained for 15 minutes following each temperature increment to ensure the stabilization of the sample temperature, after which PL spectra were recorded using the spectrometer. Time-resolved photoluminescence (TRPL) measurements were conducted using the Edinburgh FLS 1000 spectrometer equipped with an Edinburgh Instruments EPLED picosecond laser diode, with monitoring at the emission wavelength of 594 nm for $Cs_2Pb(SCN)_2I_2$ films.

Device performance measurement

Photodetection was performed utilizing a Cindbest CGO probe station equipped with a 450 nm single-mode fiber laser diode. *I-V* and *I-t* curves were recorded under vacuum conditions using a Keithley 2614B SourceMeter. Noise spectra were obtained by recording transient dark current using the buffer mode of the Keithley 2614B, followed by the fast Fourier transform of the dark current data. X-ray photons with a peak energy of 22 keV were produced using a portable silver-target X-ray generator with an aluminum collimator (outlet diameter: 5 mm). The accelerating voltage was fixed at 30 kV and the X-ray dose rate was controlled by adjusting the generator's input current (100−500 μA). The dosimeter was positioned identically to the detector for measuring the dose rate. *I*−*t* curves under X-ray irradiation were recorded using a Keithley 6517B electrometer.

Calculation method

Device's responsivity (R) and specific detectivity (D^*), R and D^* were calculated using the formulas:

$$R = \frac{I_{on} - I_d}{P \times S}$$

$$D^* = \frac{R\sqrt{S}}{\sqrt{2qI_d}}$$

where I_p, I_d, P, S, and q represent the photocurrent, dark current, light intensity, device's effective area, and elementary charge, respectively.

Device's sensitivity (S) and signal-to-noise ratio (SNR) under X-ray was calculated by linearly fitting the correlation between photocurrent and dose rate using the formula:

$$S = \frac{I_p - I_d}{D \times A}$$

$$\mathrm{SNR} = \frac{\bar{I}_p - \bar{I}_d}{\sqrt{\frac{1}{k}\sum_{i}^{k}(I_i - \bar{I}_p)^2}}$$

where I_p is the photocurrent, I_d is the dark current, S is the sensitivity, D is the dose rate, and A is the effective area of the device.

2. Supplementary data

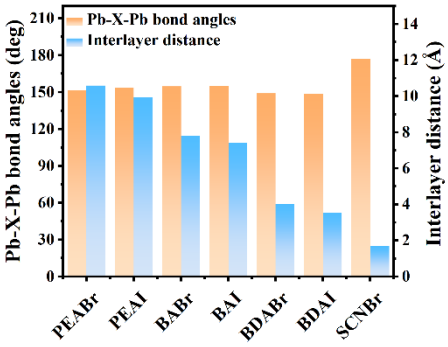

Fig. S1 Statistical plots of the average Pb-X-Pb (X = I^- or Br^-) bond angles and interlayer distance in representative 2DPKs. PEABr, PEAI, BABr, BAI, BDABr, BDAI, and SCNBr represent $(PEA)_2PbBr_4$[1], $(PEA)_2PbI_4$[2], $(BA)_2PbBr_4$[1], $(BA)_2PbI_4$[3], $BDAPbBr_4$[4], $BDAPbI_4$[5], $Cs_2Pb(SCN)_2Br_2$, respectively.

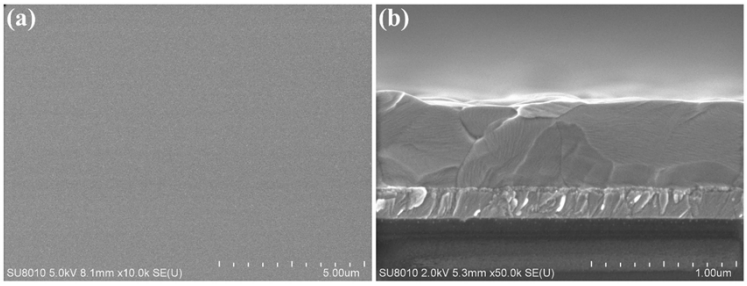

Fig. S2 Surface and cross SEM images of the $Cs_2Pb(SCN)_2I_2$ film.

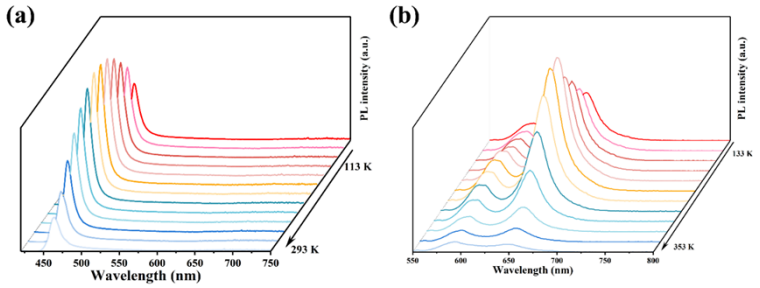

Fig. S3 Temperature-dependent PL spectra of (a) $Cs_2Pb(SCN)_2Br_2$ and (b) $Cs_2Pb(SCN)_2I_2$.

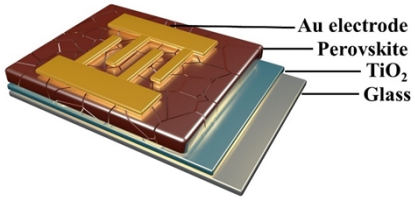

Fig. S4 Device structure schematic of Au interdigital electrode/perovskite film/TiO_2/Glass.

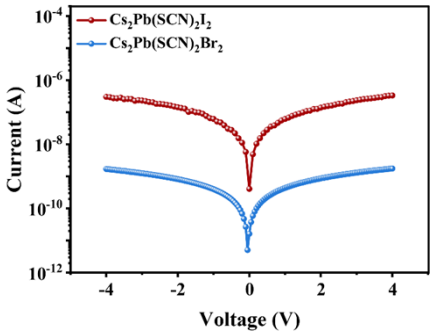

Fig. S5 *I-V* curves of $Cs_2Pb(SCN)_2Br_2$ and $Cs_2Pb(SCN)_2I_2$ devices under 405 laser illumination.

Table S1 Device performance of $(Cs)_2Pb(SCN)_2I_2$ films with different PVP concentrations.

PVP (mg mL^{-1})	I_{dark} (nA)	I_{light} (nA)	R (mA W^{-1})	D^* (× 10^{12} Jones)
0	0.004	93.89	6.48	0.38
2	0.004	270.91	18.69	1.41
4	0.005	302.41	20.83	1.40
6	0.005	218.01	1.50	1.01

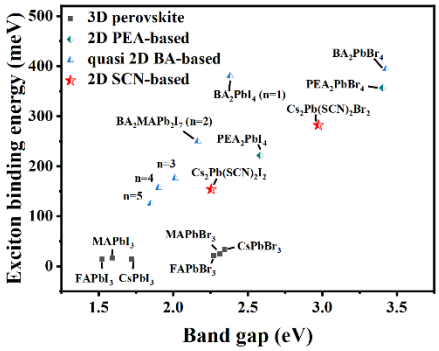

Fig. S6 Summary of exciton binding energy versus band gap curve based on reported perovskites; PEA_2PbI_4[2], PEA_2PbBr_4[1], BA_2PbI_4[3], BA_2PbBr_4[1], $BA_2MA_{n-1}Pb_nI_{3n+1}$ (n =2, 3, 4, and 5)[6], $MAPbI_3$[7], $MAPbBr_3$[8], $FAPbI_3$[7], $FAPbBr_3$[7], $CsPbI_3$[9], and $CsPbBr_3$[9].

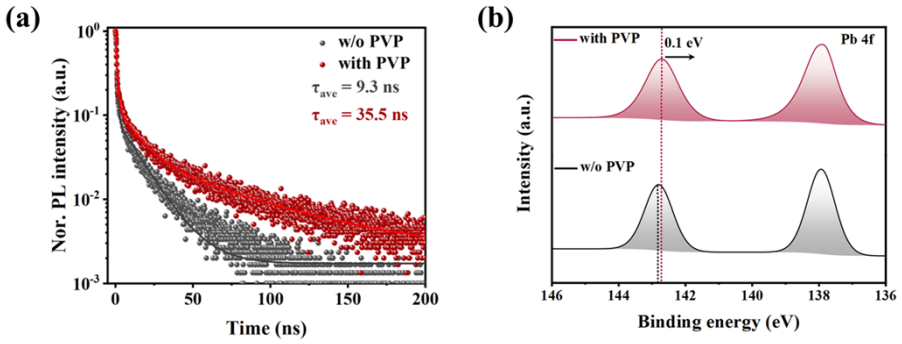

Fig. S7 (a)TRPL and (b) XPS spectra of $Cs_2Pb(SCN)_2I_2$ films with and without PVP.

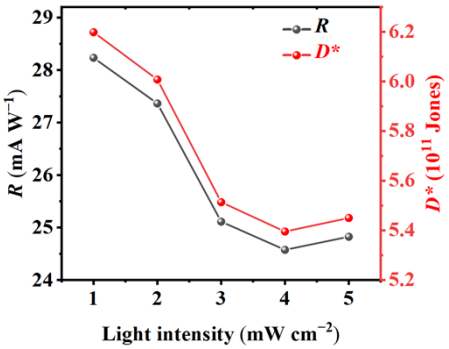

Fig. S8 *R* and *D** versus light intensity of the $Cs_2Pb(SCN)_2I_2$ device.

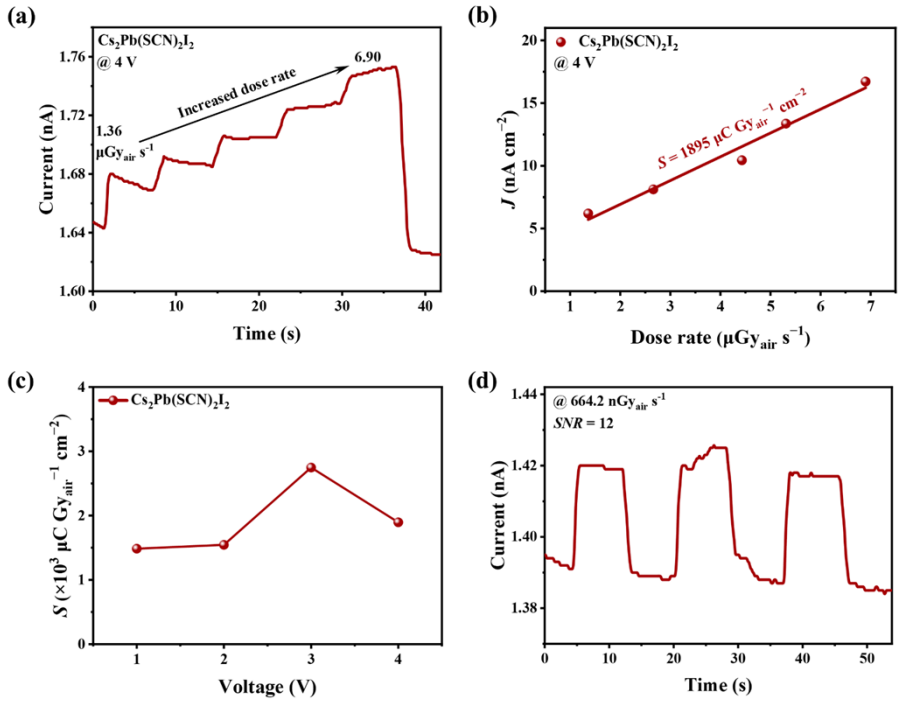

Fig. S9 (a) *I-t* curves of $Cs_2Pb(SCN)_2I_2$ devices under increased X-ray dose rates. (b) Linearly fitting the photocurrent density at different dose rates to determine device's sensitivity. (c) Sensitivity at different bias. (d) *I-t* curves of the device at low dose rate.

Table S2 Performance comparison of our 2D $Cs_2Pb(SCN)_2I_2$ film photodetector with those in published literature.

Material	Responsivity ($A\ W^{-1}$)	Detectivity (Jones)	Response speed	References
$MAPbI_3$ SC	0.15	/	120 ms	[10]
$MAPbBr_3$ SC	0.26	1.5×10^{13}	100 ns	[11]
$MAPbCl_3$ SC	0.047	1.2×10^{10}	24 ms	[12]
$CsPbBr_3$ SC	0.028	1.8×10^{11}	100 ms	[13]
$(PEA)_2PbBr_4$ SC	5.4×10^{-3}	1.07×10^{13}	/	[14]
$Cs_2Pb(SCN)_2Br_2$ SC	8.5×10^{-3}	1.2×10^{10}	2.6 ms	[15]
$MAPbI_3$ film	0.11	1.3×10^{11}	20 ms	[16]
$MAPbCl_3$ film	0.071	2.87×10^{10}	/	[17]
$MAPbICl_2$ film	0.67	1.4×10^{13}	200 ms	[18]
$Cs_2Pb(SCN)_2I_2$ film	0.028	6.2×10^{11}	2.78 ms	This work

Table S3 X-ray detection performance of different perovskite devices.

Material	SC/film	Source energy	Sensitivity ($\mu C\ Gy_{air}^{-1}\ cm^{-2}$)	Detectable limit ($\mu\ Gy_{air}\ s^{-1}$)	Ref
α-Se	film	20 keV	20	5.5	[19]
Si	SC	8 MeV	8	< 8300	[20]
CZT	film	80 keV	318	50	[21]
$MAPbBr_3$	SC	22 keV	80	0.5	[22]
$(F–PEA)_2PbI_4$	SC	120 keV	3402	0.023	[23]
$Cs_3Bi_2I_9$	SC	40 kV	1652.3	0.13	[24]
$Cs_2AgBiBr_6$	SC	30 keV	105	0.059	[25]
$MAPbI_3$	film	37 keV	1.5	N/A	[26]
$CsPbBr_3$	film	30 keV	55684	0.215	[27]
Cs_2TeI_6	film	20 kV	76.27	0.17	[28]
$CsPbI_2Br$	film	30 keV	120	0.026	[29]
$Cs_2Pb(SCN)_2I_2$	film	22.2 keV	2747	0.664	This work

References

1. H. Takagi, H. Kunugita and K. Ema, *Phys. Rev. B*, 2013, **87**, 125421.
2. X. Hong, T. Ishihara and A. V. Nurmikko, *Phys. Rev. B*, 1992, **45**, 6961-6964.
3. X. Chen, H. Lu, K. Wang, Y. Zhai, V. Lunin, P. C. Sercel and M. C. Beard, *J. Am. Chem. Soc.*, 2021, **143**, 19438-19445.
4. M. D. Smith, A. Jaffe, E. R. Dohner, A. M. Lindenberg and H. I. Karunadasa, *Chem. Sci.*, 2017, **8**, 4497-4504.
5. A. Lemmerer and D. G. Billing, *CrystEngComm*, 2012, **14**, 1954-1966.
6. J. C. Blancon, A. V. Stier, H. Tsai, W. Nie, C. C. Stoumpos, B. Traoré, L. Pedesseau, M. Kepenekian, F. Katsutani, G. T. Noe, J. Kono, S. Tretiak, S. A. Crooker, C. Katan, M. G. Kanatzidis, J. J. Crochet, J. Even and A. D. Mohite, *Nat. Commun.*, 2018, **9**, 2254.
7. K. Galkowski, A. Mitioglu, A. Miyata, P. Plochocka, O. Portugall, G. E. Eperon, J. T.-W. Wang, T. Stergiopoulos, S. D. Stranks, H. J. Snaith and R. J. Nicholas, *Energy Environ. Sci.*, 2016, **9**, 962-970.
8. Q. Wang, X.-D. Liu, Y.-H. Qiu, K. Chen, L. Zhou and Q.-Q. Wang, *AIP Advances*, 2018, **8**.
9. Z. Yang, A. Surrente, K. Galkowski, A. Miyata, O. Portugall, R. J. Sutton, A. A. Haghighirad, H. J. Snaith, D. K. Maude, P. Plochocka and R. J. Nicholas, *ACS Energy Lett.*, 2017, **2**, 1621-1627.

10. C. Bao, Z. Chen, Y. Fang, H. Wei, Y. Deng, X. Xiao, L. Li and J. Huang, *Adv. Mater.*, 2017, **29**, 1703209.
11. C. Bao, Z. Chen, Y. Fang, H. Wei, Y. Deng, X. Xiao, L. Li and J. Huang, *Adv. Mater. 2017, 29, 1703209*, 2017, **29**, 1703209.
12. G. Maculan, A. D. Sheikh, A. L. Abdelhady, M. I. Saidaminov, M. A. Haque, B. Murali, E. Alarousu, O. F. Mohammed, T. Wu and O. M. Bakr, *J. Phys. Chem. Lett.*, 2015, **6**, 3781-3786.
13. O. Almora, G. J. Matt, A. These, A. Kanak, I. Levchuk, S. Shrestha, A. Osvet, C. J. Brabec and G. Garcia-Belmonte, *The Journal of Physical Chemistry Letters*, 2022, **13**, 3824-3830.
14. C.-H. Lin, B. Cheng, T.-Y. Li, J. R. D. Retamal, T.-C. Wei, H.-C. Fu, X. Fang and J.-H. He, *ACS Nano*, 2019, **13**, 1168-1176.
15. C. H. Liao, C. H. Chen, J. Bing, C. Bailey, Y. T. Lin, T. M. Pandit, L. Granados, J. Zheng, S. Tang, B. H. Lin, H. W. Yen, D. R. McCamey, B. J. Kennedy, C. C. Chueh and A. W. Y. Ho Baillie, *Adv. Mater.*, 2022, **34**, 2104782.
16. K. C. Kwon, K. Hong, Q. Van Le, S. Y. Lee, J. Choi, K.-B. Kim, S. Y. Kim and H. W. Jang, *Adv. Funct. Mater.*, 2016, **26**, 4213-4222.
17. E. Zheng, B. Yuh, G. A. Tosado and Q. Yu, *J. Mater. Chem. C*, 2017, **5**, 3796-3806.
18. F. Cao, W. Tian, B. Gu, Y. Ma, H. Lu and L. J. N. R. Li, *Nano Res.*, 2017, **10**, 2244-2256.
19. S. O. Kasap, *J. Phys. D*, 2000, **33**, 2853.
20. M. Guerra, M. Manso, S. Longelin, S. Pessanha and M. L. Carvalho, *J. Instrum.*, 2012, **7**, C10004.
21. Y. M. Ivanov, V. M. Kanevsky, V. F. Dvoryankin, V. V. Artemov, A. N. Polyakov, A. A. Kudryashov, E. M. Pashaev and Z. J. Horvath, *Phys. Stat. Sol. C*, 2003, **0**, 840-844.
22. H. Wei, Y. Fang, P. Mulligan, W. Chuirazzi, H.-H. Fang, C. Wang, B. R. Ecker, Y. Gao, M. A. Loi, L. Cao and J. Huang, *Nat. Photonics*, 2016, **10**, 333-339.
23. H. Li, J. Song, W. Pan, D. Xu, W.-a. Zhu, H. Wei and B. Yang, *Adv. Mater.*, 2020, **32**, 2003790.
24. Y. Zhang, Y. Liu, Z. Xu, H. Ye, Z. Yang, J. You, M. Liu, Y. He, M. G. Kanatzidis and S. Liu, *Nat. Commun.*, 2020, **11**, 2304.
25. W. Pan, H. Wu, J. Luo, Z. Deng, C. Ge, C. Chen, X. Jiang, W.-J. Yin, G. Niu, L. Zhu, L. Yin, Y. Zhou, Q. Xie, X. Ke, M. Sui and J. Tang, *Nat. Photonics*, 2017, **11**, 726-732.
26. S. Yakunin, M. Sytnyk, D. Kriegner, S. Shrestha, M. Richter, G. J. Matt, H. Azimi, C. J. Brabec, J. Stangl, M. V. Kovalenko and W. Heiss, *Nat. Photonics*, 2015, **9**, 444-449.
27. W. Pan, B. Yang, G. Niu, K. H. Xue, X. Du, L. Yin, M. Zhang, H. Wu, X. S. Miao and J. Tang, *Adv. Mater.*, 2019, **31**, 1904405.
28. J. Guo, Y. Xu, W. Yang, B. Xiao, Q. Sun, X. Zhang, B. Zhang, M. Zhu and W. Jie, *ACS Appl. Mater. Interfaces*, 2021, **13**, 23928-23935.
29. P.-T. Lai, H.-C. Lin, Y.-T. Chuang, C.-Y. Chen, W.-K. Cheng, G.-H. Tan, B.-W. Hsu, L. Yang, S.-C. Lou, L.-J. Chien, H.-W. Wang and H.-W. Lin, *ACS Appl. Mater. Interfaces*, 2022, **14**, 19795-19805.